Advances in Technology, Staining Protocol, and Flattening Devices in Ex Vivo Confocal Microscopy

Javiera Pérez-Anker, Susana Puig, and Josep Malvehy

16.1 Introduction

Since the development of confocal microscopy technology in 1957, a long journey has brought us to the analysis of digital images of hematoxylin and eosin, and artificial intelligence as applied to the field of histology. Progress in ex vivo confocal microscopy technology now allows immediate visualization of freshly excised tissue, in less than 3 min and at the bedside. This instant diagnosis has opened the door to significant progress in the field of dermatology and also in general pathology [1–4].

Not all the journey has been easy and represents more than 20 years of continuous progress. From a slow device with white and gray images divided into squares, to a fast device with real-time digital hematoxylin and eosin (H&E) images obtained by strip mosaicking, this road began with one modest first step (Fig. 16.1). Technology, as applied to ex vivo confocal microscopy, has steadily improved over the years. Furthermore, not only has the technology changed, but staining methods have also changed over time, along with methods of preparing the specimen to be scanned [4] (Table 16.1).

16.2 Reflectance Confocal Microscopy in Ex Vivo Confocal Microscopy

The first published results in ex vivo confocal microscopy (evCM) for clinical applications were in 2001, by Milind Rajadhyaksha and Salvador González [5]. A similar technique was described in 1995, for in vivo confocal microscopy (ivCM) by Rajadhyaksha et al. [6] and was applied for the analysis of evCM images.

These images were obtained by two reflectance confocal microscopes. The authors stained the nuclei with acetic acid at 5% in order to enhance the contrast by whitening the skin component and compacting the chromatin. A laser of 1064 nm wavelength allowed deep visualization of the tissue, in spite of a lower quality resolution of the structures.

In 2003, a new commercialized device only for ex vivo purposes (VivaScope 2000s, Lucid Inc., NY, USA), with an 830 nm diode laser (a reflectance laser) and a 30X objective lens, was utilized to evaluate discarded tissue from the first stage of Mohs surgery operations on basal cell carcinomas and squamous cell carcinomas. Acetic acid at 5% was utilized as a stain contrast with better results than reported in previous studies [7]. A real-time image visualization for Mohs surgery was achieved.

In 2007, the same pioneer group which created the first confocal created a mosaic of 15×15 mm (equivalent to a 2X view of macroscopic image) in 9 min [8]. They also realized that the flattening of the tissue was fundamental to visualizing all the structures during the scanning. A flattening device consisting of an Agarose 3% gel disk, 2 mm thick was proposed for the first time. The gel disk was placed on top of the specimen inside a piston housing of polycarbonate. A piston compressed the gel and the specimen on the slide, achieving a uniformly flattened specimen. Visualization of the tissue was greatly improved.

Staining methods also changed in 2009 when a German group proposed the use of Citric acid 10% for 2 min, scanning with the VS2500, observing the images in reflectance mode [9].

16.3 Fluorescence Confocal Microscopy for Ex Vivo Confocal Microscopy

Another radical change occurred in 2009 when the use of a fluorescent laser (445 nm) was proposed for Mohs surgery [10]. The staining method also varied, and the use of

J. Pérez-Anker (✉) · S. Puig · J. Malvehy
Dermatology Department, Hospital Clinic de Barcelona, Carrer de Villarroel, 170, Barcelona, 08036, España
e-mail: perez12@clinic.cat
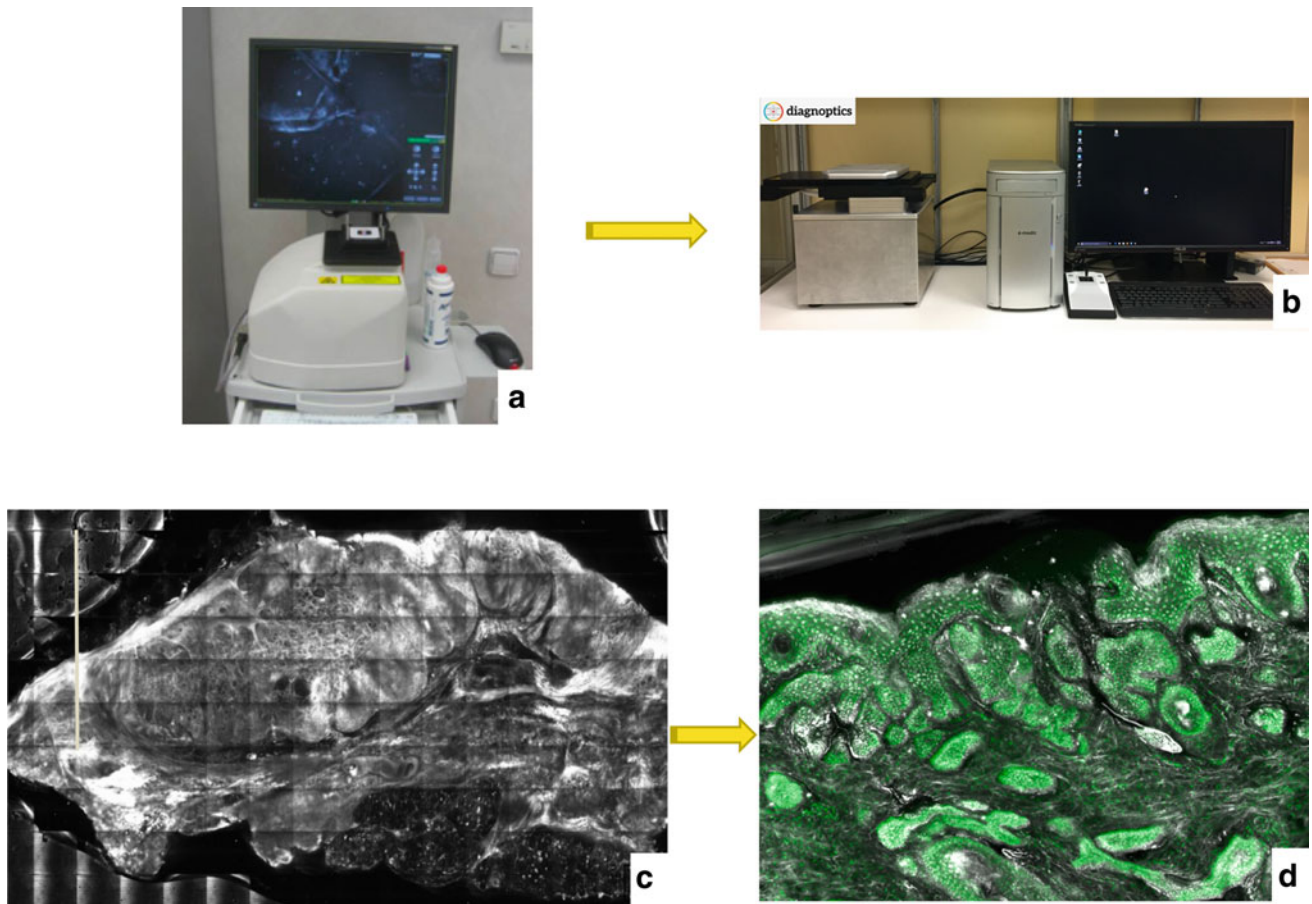
Fig. 16.1 Progression of evCM microscopes. **a** VS2500 Gen3. **b** Diagnoptics prototype. **c** Nodular basal cell carcinoma image obtained by VS2500 Gen3 with reflectance laser. **d** Infiltrating basal cell carcinoma image obtained by VS2500 Diagnoptics prototype with fusion mode and strip mosaicking.

Table 16.1 Evolution of Vivascope® devices

Device	Year	Laser	Mode	Scan area	Acquisition	Objective	FOV	Time
VS2000	2001	1064 nm	Reflectance		Mosaic	10, 20, 30, 60, 100X	150–2000 μm	5–6.5 min
VS2000	2003	830 nm	Reflectance	10 × 10 mm	Mosaic	30X	750 μm	
VS2500 Gen2	2009	830 nm 658 nm 445 nm	Reflectance Fluorescence Fluorescence	16 × 16 mm	Mosaic	25X	750 μm	9 min
VS2500 Gen2	2010	830 nm 658 nm 488 nm	Reflectance Fluorescence Fluorescence	16 × 16 mm	Mosaic	25X	750 μm	
VS2500 Gen3	2014	830 nm 658 nm 488 nm	Reflectance Fluorescence Fluorescence	20 × 20 mm	Mosaic	25X	635 μm	
VS2500 Gen4	2018	785 nm 488 nm	Reflectance Fluorescence	25 × 25 mm	Strip	38X	500 μm	
VS2500 Gen4	2020	638 nm 488 nm	Reflectance Fluorescence	25 × 25 mm	Strip	38X	500 μm	2–3 min

acridine orange was introduced in the preparation of the sample. Only a fluorescent laser was utilized.

Since 2010, a fluorescence 488 nm laser has been used in most published studies, and the technology has not changed significantly. Although the device could employ a fluorescent 658 nm laser or a reflectance 830 nm laser, investigators have, in general, preferred using acridine orange and a continuous wave 488 nm laser. A great deal of evidence has been accumulated in favor of safety in the use of this device and technique [3, 10–19].

Simultaneously, another device called HistoLog scanR FCM® was developed which allowed the visualization of larger images than the other devices 8 × 8 cm. The final image of the scanned tissue can be seen in digital purple, using only a 488 nm laser [4] (Table 16.2).

In 2007, efficacy in the visualization of tumoral islands of basal cell carcinoma was compared between the three different lasers available at that time: two fluorescent lasers (633 and 656 nm) and a reflectance laser (830 nm). In addition, new contrast agents were proposed: methylene blue 1% and toluidine blue 1%.

16.4   Fusion Mode: Simultaneous Fluorescence + Reflectance

In 2016, the authors of this chapter analyzed different benign and malignant lesions using fluorescence and reflectance lasers, with a new staining protocol of acetic acid and acridine orange, using the VS2500 Gen2 (Figs. 16.2 and 16.3) [20].

Since then, other European authors have also compared different visualization features in both lasers as applied to diverse skin lesions [21–23].

Regarding the flattening of the tissue, in 2017, another option appeared in an attempt to improve the representativeness of the sample. This system consisted of a plastic slide with grub screws that covered the specimen.

Unfortunately, this method was time-consuming and rapid tissue visualization is essential [24].

The basis of the fusion mode 4th generation VivaScope device (the latest generation of confocal microscopy) consists in scanning with two different lasers (fluorescence and reflectance) at the same time, strip mosaicking and subsequently, the analysis of digital images of hematoxylin and eosin.

The first time that two different lasers, fluorescence (488 nm) and reflectance (830 nm), scanned at the same time was with a prototype developed in 2005 [25]. In this study, in vivo confocal images were correlated with ex vivo conventional microscopy images.

Another substantial change occurred in 2011 when the strip mosaicking in ratios of 10:1 instead of ∼1:1 was obtained and stitched together using novel software [26]. With this technology, an area of 10 × 10 mm was scanned in about 3 min—3 times as fast asthe previous method.

16.5   Fusion Mode with Strip Mosaicking and Digital H&E

In 2009, the third revolutionary technological advance was initiated: for the first time, confocal ex vivo digital images of H&E could be observed, simulating real histopathology slides. The visualization was rendered by two lasers (according to the described prototype where both fluorescent and reflectance lasers were used simultaneously) and using software to change the initial colors of the scanned images: the reflectance mosaic was digitally changed to pink and the fluorescence mosaic to purple. This was the last significant step to the technology that is available today together with the improvement of the software compared to the first method of digital H&E staining in evCM [27, 28].

A further step was taken in 2016 when the authors of this chapter started to work with a prototype in the context of a European consortium called Diagnoptics (Fig. 16.4). The device was a prototype that scanned simultaneously in

Table 16.2 Comparison of evCM devices. Adapted from Malvehy et al. [4].

System	HistoLog scanR FCM®	Vivascope2500M-G4R FCM®
Modality of CM Image area (max)	FCM	FCM + +RCM
Image area (max)	8 × 8 cm	2.5 × 2.5 cm
Laser	488 nm	785 nm + 488 nm
Scanning characteristics	1600 × 1600 to 8000 × 8000 pixels	1024 × 1024 pixels Optical section thickness = 4 μm Depth of scanning <200 μm Magnification up to 540x
Display of images	Purple digital color	Green (FCM)/ Gray scale (RCM); Fusion green-gray; H&E digital staining Table
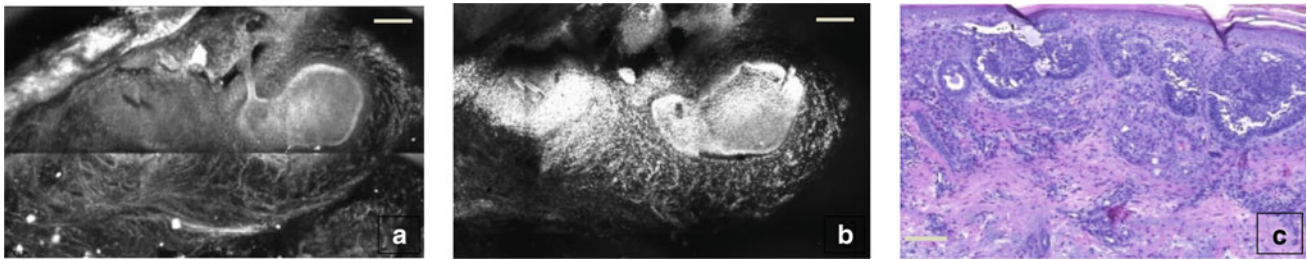
Fig. 16.2. VS2500 Gen2 scanned image of a superficial BCC stained with Acridine orange 0.1 mmol L[1] + acetic acid 50%. Different stromal reactions were observed in each laser. **a** Reflectance laser. **b** Fluorescence laser. **c** H&E [20]

Fig. 16.3. Nuclear visualization with different stain protocols [30]. Nodular basal cell carcinoma using reflectance laser. Image obtained by VS2500 Diagnoptics prototype with fusion mode and strip mosaicking. **a** Acridine orange 0.1 mmol L[1] + acetic acid 50%. **b** Acridine orange 0.1 mmol L[1] [20]
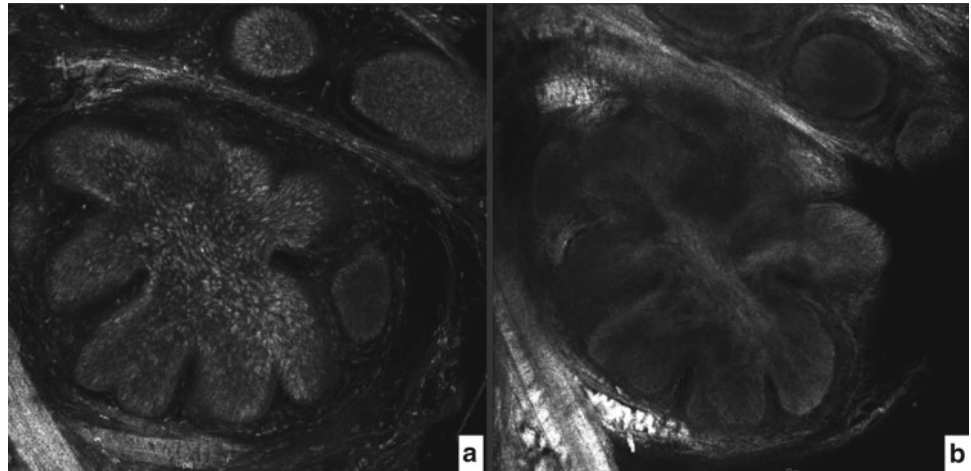
reflectance and fluorescence modes and used the strip mosaicking software to integrate the captured images (Fig. 16.4) [29]. Differences between fluorescence, reflectance, and fusion laser mode and also a comparison between the different staining methods were described for basal cell carcinoma [20, 30].

With a few changes suggested by the study group, the algorithm put forward by Gareau et al. [27] was integrated into the new version of the commercial machine and the VS 4th Gen appeared on the market in 2018 (Figs. 16.4, 16.5, 16.6, 16.7, 16.8, 16.9, 16.10 and 16.11) [29–33].

16.6 New Staining Protocols

A new staining method was also suggested, combining the benefits of acetic acid and acridine orange staining (Table 16.3) (Figs. 16.3, 16.4, 16.5, 16.6, 16.7, 16.8, 16.9, 16.10 and 16.11).

The next significant change was suggested by the authors regarding flattening methods [34] and steps were suggested

to obtain a good image with this technique (also described in Chap. 3) [35]. In addition to mechanical flattening methods, recently, Sendin-Martin et al. [36] demonstrated a digital approach to flatten excised Mohs margin tissue for complete visualization of epidermal margin.

The greatest advantage of applying digital H&E is that the diagnostic criteria normally applied in different histological diagnoses can also be visualized and applied in the diagnosis with ex vivo confocal microscopy [4, 37–39]. This has previously been demonstrated by the authors of this chapter, and the feature visualization of the structures, only in fluorescence or reflectance mode, is now utilized to differentiate doubtful areas of the image of the scanned tissue [4, 37–39].

The new generation of ex vivo confocal microscopy has led to a revolution in the field of diagnosis and histology-driven treatment. New applications in other fields of general pathology have also quickly begun to appear [1, 2, 40] and pathologists have been able to increase their confidence in diagnosis using ex vivo confocal microscopy with digital hematoxylin and eosin.
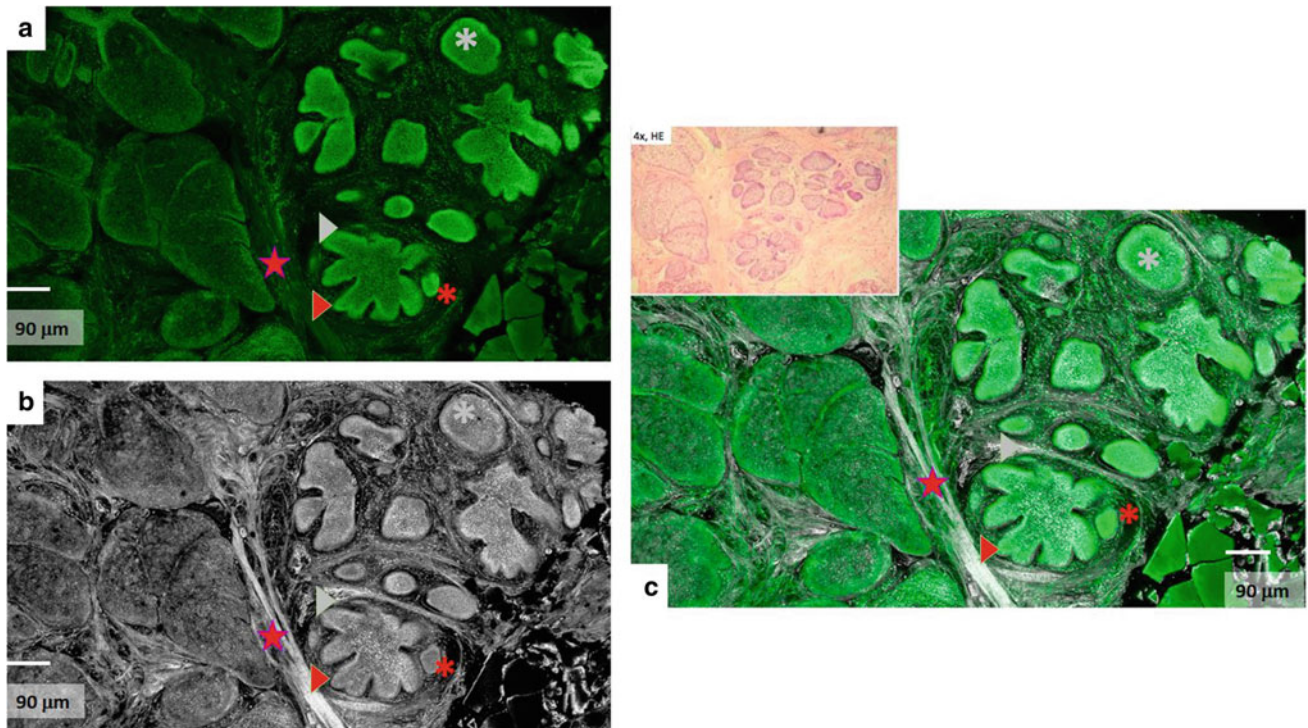
Fig. 16.4. Diagnoptics prototype scanned image of a nodular BCC stained with Acridine orange 0.1 mmol L^1 + acetic acid 50%. **a** Fluorescence laser. **b** Reflectance laser. **c** Fusion image (simultaneous fluorescence an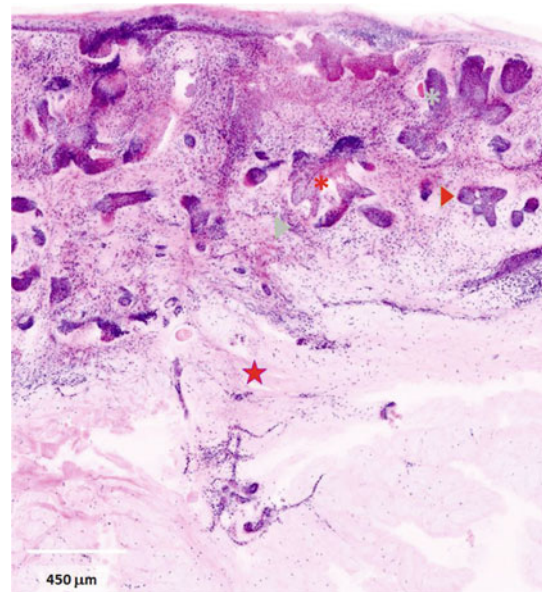d reflectance lasers) and H&E. Histological features can be recognized: clefting (red asterisk), palisading (red triangle), nuclear pleomorphism and increased nuclear/cytoplasm ratio (gray asterisk), peri-tumoral stromal reaction (gray triangle), thickened collagen bundles (red star) [30]

Fig. 16.5. VivaScope® 2500 MM-Gen4 digital H&E scanned image of a nodular BCC, previously prepared with Acridine orange 0.1 mmol L^1 + acetic acid 50%. Histological features can be recognized: clefting (red asterisk), palisading (red triangle), thickened collagen bundles (red star) [4, 30, 36–38]
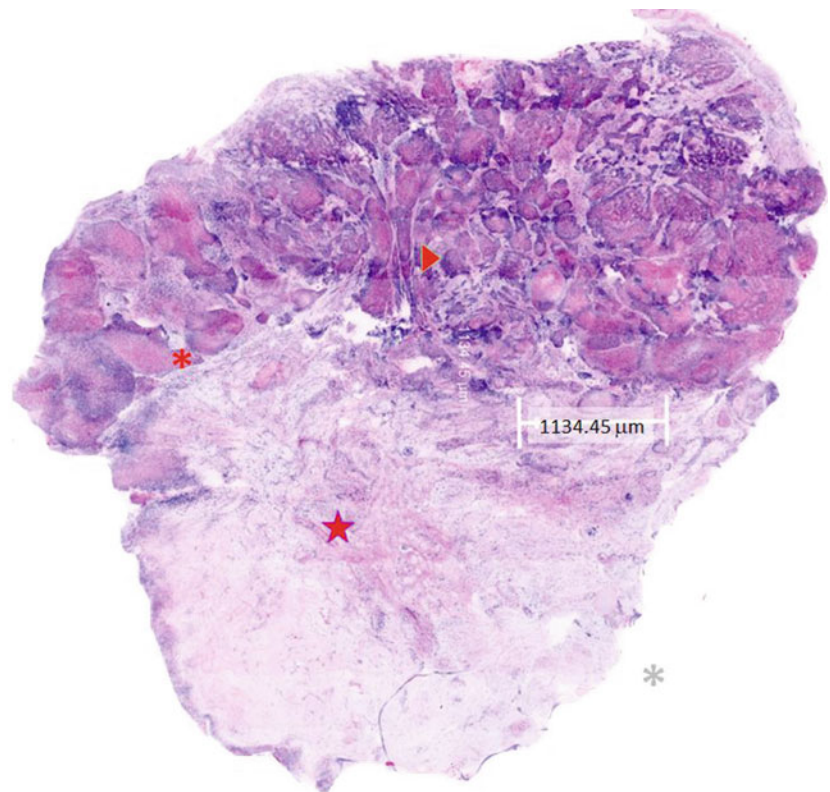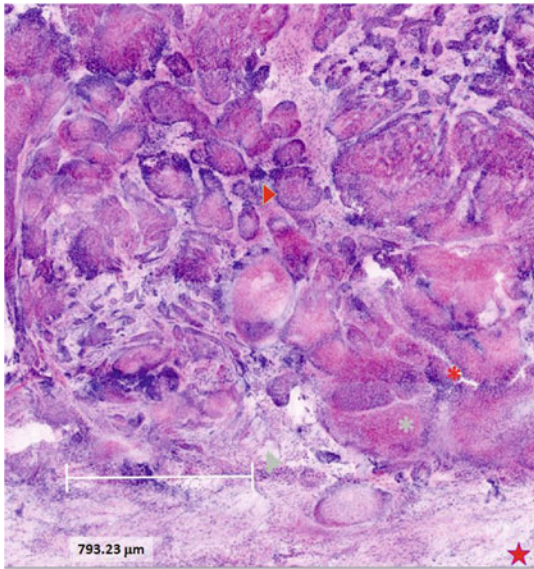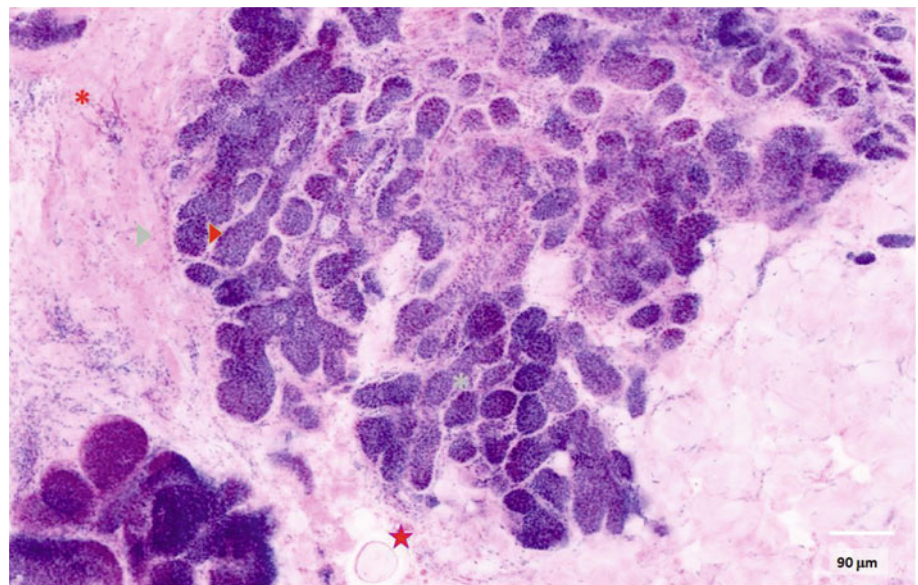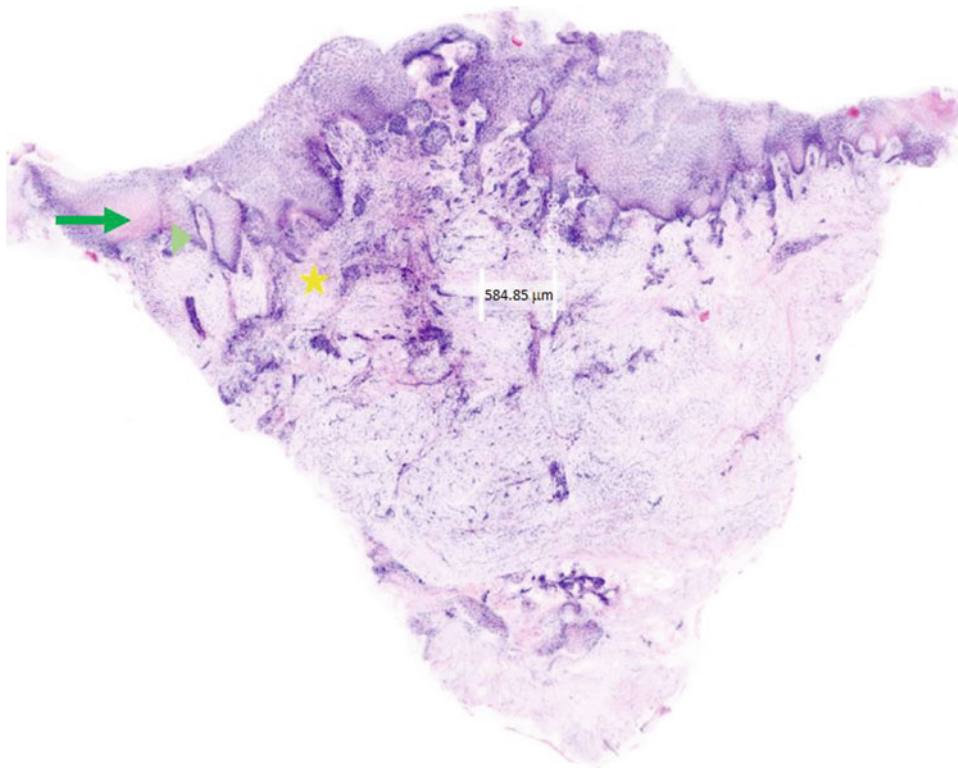
Fig. 16.6. VivaScope® 2500 MM-Gen4 digital H&E scanned detail image of a nodular BCC previously prepared with Acridine orange 0.1 mmol L^1 + acetic acid 50%. Histological features can be recognized: clefting (red asterisk), palisading (red triangle), nuclear pleomorphism and increased nuclear/cytoplasm ratio (gray asterisk), peri-tumoral stromal reaction (gray triangle), thickened collagen bundles (red star) [4, 30, 36–38]

Fig. 16.7. VivaScope® 2500 MM-Gen4 digital H&E scanned detail image of an infiltrating BCC previously prepared with Acridine orange 0.1 mmol L^1 + acetic acid 50%. Histological features can be recognized: clefting (red asterisk), palisading (red triangle), nuclear pleomorphism and increased nuclear/cytoplasm ratio (gray asterisk), peri-tumoral stromal reaction (gray triangle), thickened collagen bundles (red star) [4, 30, 36–38]

Fig. 16.8. VivaScope® 2500 MM-Gen4 digital H&E scanned detail image of a micronodular BCC previously prepared with Acridine orange 0.1 mmol L^1 + acetic acid 50%. Histological features can be recognized: clefting (red asterisk), palisading (red triangle), nuclear pleomorphism and increased nuclear/cytoplasm ratio (gray asterisk), peri-tumoral stromal reaction (gray triangle), thickened collagen bundles (red star) [4, 30, 36–38]
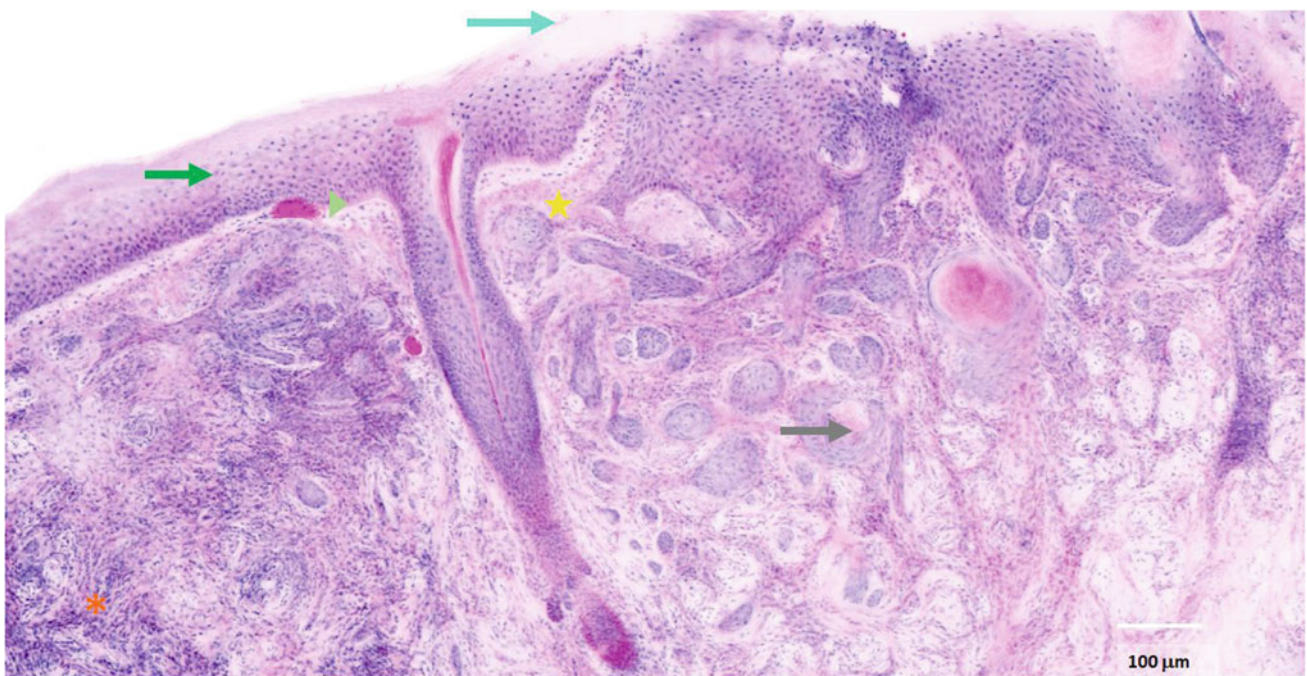
Fig. 16.9. VivaScope® 2500 MM-Gen4 digital H&E scanned image of an infiltrating SCC previously prepared with Acridine orange 0.1 mmol L[1] + acetic acid 50%. Histological features can be recognized. Epidermis (dark green arrow), DEJ (light green triangle), dermis (yellow asterisk) [4, 30, 36–38]

Fig. 16.10. VivaScope® 2500 MM-Gen4 digital H&E scanned detail image of an infiltrating SCC previously prepared with Acridine orange 0.1 mmol L[1] + acetic acid 50%. Full macroscopic histological features can be seen. Epidermis (dark green arrow), DEJ (light green triangle), dermis (yellow asterisk), keratin pearls (light gray arrow), parakeratosis (turquoise arrow), inflammatory cells (dark orange asterisk) [4, 30, 36–38]
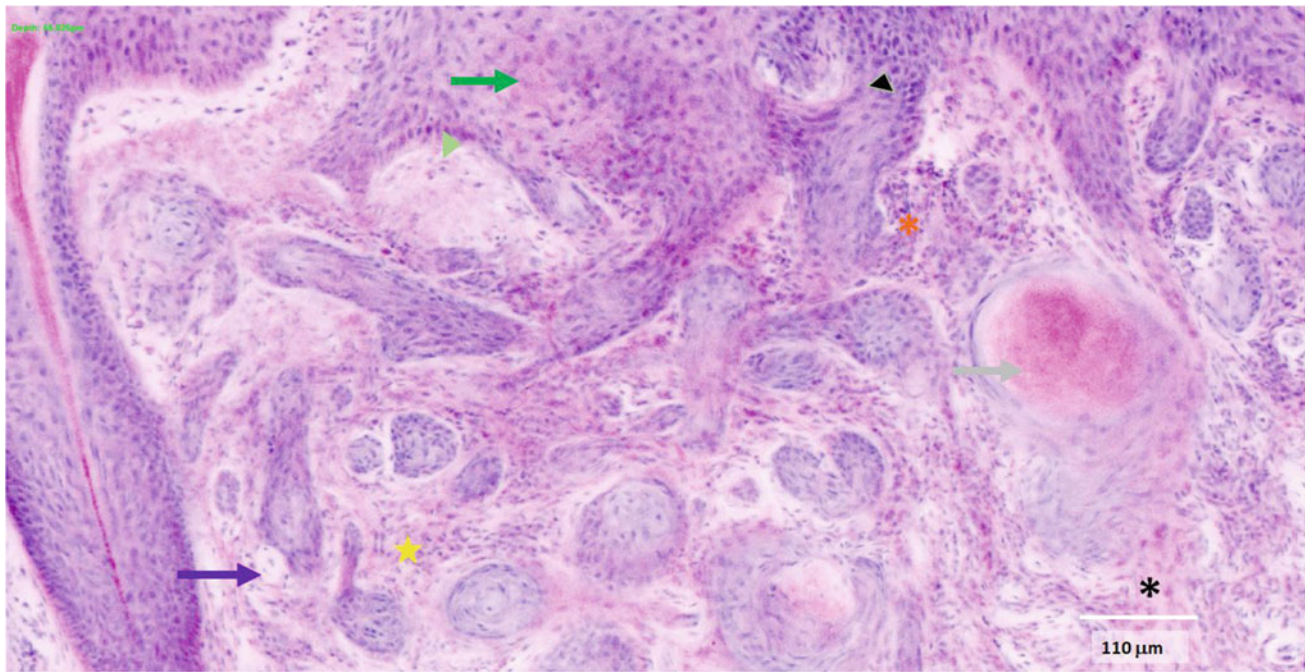
Fig. 16.11. Detail image of infiltrating SCC. Full microscopic histological features can be seen. Epidermis (dark green arrow), DEJ (light green triangle), dermis (yellow star), vessels (purple arrow), keratin pearls (light gray arrow), cellular atypia (black triangle), dyskeratotic cells (black asterisk), inflammatory cells (dark orange asterisk) [4, 36–38]

Table 16.3 Staining methods for ex vivo CM and application in dermatology. RCM: reflectance confocal microscopy; FCM: fluorescence confocal microscopy; M-CM: multimodal confocal microscopy. Adapted from Malvehy et al. [4].

| Staining agent	Laser	Sample
Aluminum chloride, acetic acid, citric acid	RCM	Skin tumors
Acridine orange, methylene blue, and toluidine blue, fluorescein, Nile blue, or Patent Blue V	FCM	Skin tumors
Combinations	**Laser**	**Sample**
Methylene blue + toluidine blue	M-CM	Skin cancer
Fluorescence proflavine + acetic acid + oluidine blue	FCM	BCC
Acetic acid + Acridine orange	M-CM	BCC
Acridine orange + ethidium bromide	3-color FCM	BCC
Immunostaining	**Laser**	**Sample**
FITC-labeled S-100A10, Melan-A, and anti-Ber-EP4 antibodies, NPs10@D1_ICF_Alexa647_ DOTAGA Fe3 +	FCM	No-melanocytic and melanocytic tumors
Fluorescent-labeled IgG and C3 antibodies	M-CM	Bullous pemphigoid
IgG, IgM, IgA, C3, and Fibrinogen	M-CM	Cutaneous vasculitis

16.7 Artificial Intelligence Color and Image Interpretation

Progress toward this method started through experimenting with artificial intelligence. Marc Combalia et al. proposed digital staining through deep learning [41], with digital colors almost equal to regular H&E that may have clinical applicability in the future (Fig. 16.12). As with digital pathology, AI will have a role in diagnosis in evCM, assessment of tumor margins, and in other applications. However, validation of machine learning needs to be done in this field to prove its clinical usability.

To summarize, the technology for evCM has evolved steadily over recent years. The core technology has been miniaturized in different devices and new lasers have been developed, bringing fluorescence capability instead of only reflectance mode (830 nm). Fusion images of evRCM and
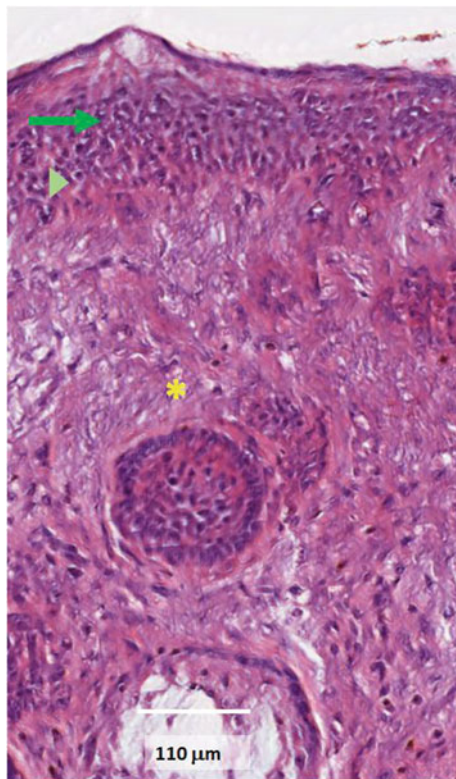
Fig. 16.12. VivaScope® 2500 M-Gen4 AI stained scanned detail image of normal skin previously prepared with Acridine orange 0.1 mmol L^1 + acetic acid 50%. Microscopic histological features can be recognized. Epidermis (dark green arrow), DEJ (light green triangle), dermis (yellow asterisk) [40]

evFCM and digital H&E staining render high-quality pathological images similar to standard digital pathology. Moreover, the most recent changes have been the incorporation of a macroscopic camera and also the implementation of strip mosaicking (V2500 Gen4). Furthermore, the first device (VS2000), built in 2003 from the prototype developed by Rajadhyaksha in 2001, had a 25X objective, and the latest generation uses 38X, increasing the resolution from previous models. Additionally, the field of view of the VS2000 was 750 µm and the maximum scan area was 10×10 mm compared to $30 \times 3 \, 0$ mm.

The very first efforts made by Rajadhyaksha and González and their team in 2001 have, twenty years later, resulted in fast, efficient, revolutionary technology that is radically changing the traditional method of processing histological samples.

References

1. Panarello D, Compérat E, Seyde O, Colau A, Terrone C, Guillonneau B. Atlas of ex vivo prostate tissue and cancer images using confocal laser endomicroscopy: a project for intraoperative positive surgical margin detection during radical prostatectomy. Eur Urol Focus. 2019;1–18.
2. Villarreal JZ, Pérez-Anker J, Puig S, Pellacani G, Solé M, Malvehy J, et al. Ex vivo confocal microscopy performs real-time assessment of renal biopsy in non-neoplastic diseases. J Nephrol [Internet]. 2020;(0123456789). Available from: https://doi.org/10.1007/s40620-020-00844-8
3. Ragazzi M, Longo C, Piana S. Ex Vivo (fluorescence) confocal microscopy in surgical pathology: state of the art, vol. 23, Advances in Anatomic Pathology. 2016; pp. 159–69.
4. Malvehy J, Pérez-Anker J, Toll A, Pigem R, García A, Alós L, et al. Ex vivo Confocal Microscopy: revolution in fast pathology in dermatology. Br J Dermatol. 2020;183(6):1011–25.
5. Rajadhyaksha M, Menaker G, Flotte T, Dwyer PJ, González S. Confocal examination of nonmelanoma cancers in thick skin excisions to potentially guide mohs micrographic surgery without frozen histopathology. J Investig Dermatol. 2001;117(5):1137–43.
6. Rajadhyaksha M, Grossman M, Esterowitz D, Webb RH, Anderson RR. In vivo confocal scanning laser microscopy of human skin: Melanin provides strong contrast. J Invest Dermatol. 1995; 104:946–52.
7. Chung VQ, Dwyer PJ, Nehal KS, Rajadhyaksha M, Menaker GM, Charles C, et al. Use of ex vivo confocal scanning laser microscopy during Mohs Surgery for Nonmelanoma Skin Cancers. Dermatol Surg. 2004;30(12p1):1470–8.
8. Patel YG, Nehal KS, Aranda I, Li Y, Halpern AC, Rajadhyaksha M. Confocal reflectance mosaicing of basal cell carcinomas in Mohs surgical skin excisions. J Biomed Optics. 2007;12 (3):034027.
9. Schüle D, Breuninger H, Schippert W, Dietz K, Moehrle M. Confocal laser scanning microscopy in micrographic surgery (three-dimensional histology) of basal cell carcinomas. Br J Dermatol. 2009;161(3):698–700.
10. Karen JK, Gareau DS, Dusza SW, Tudisco M, Rajadhyaksha M, Nehal KS. Detection of basal cell carcinomas in Mohs excisions with fluorescence confocal mosaicing microscopy. Br J Dermatol. 2009;160(6):1242–50.
11. Longo C, Ragazzi M, Castagnetti F, Gardini S, Palmieri T, Lallas A, et al. Inserting ex vivo fluorescence confocal microscopy perioperatively in mohs micrographic surgery expedites bedside assessment of excision margins in recurrent basal cell carcinoma. Dermatology. 2013;227(1):89–92.
12. Dobbs JL, Ding H, Benveniste AP, Kuerer HM, Krishnamurthy S, Yang W, et al. Feasibility of confocal fluorescence microscopy for real-time evaluation of neoplasia in fresh human breast tissue. J Biomed Optics. 2013;18(10):106016.
13. Bennàssar A, Carrera C, Puig S, Vilalta A, Malvehy J. Fast evaluation of 69 basal cell carcinomas with ex vivo fluorescence confocal microscopy: criteria description, histopathological correlation, and interobserver agreement. JAMA dermatology (Chicago, Ill). 2013;149(7):1–8.

14. Bennàssar A, Vilata A, Puig S, Malvehy J. Ex vivo fluorescence confocal microscopy for fast evaluation of tumour margins during Mohs surgery. Br J Dermatol. 2014;170(2):360–5.

15. Longo C, Ragazzi M, Rajadhyaksha M, Nehal K, Bennassar A, Pellacani G, et al. In Vivo and Ex Vivo confocal microscopy for dermatologic and mohs surgeons. Dermatol Clin. 2016;34(4):497–504.

16. Longo C, Rajadhyaksha M, Ragazzi M, Nehal K, Gardini S, Moscarella E, et al. Evaluating ex vivo fluorescence confocal microscopy images of basal cell carcinomas in Mohs excised tissue. Br J Dermatol. 2014;171(3):561–70.

17. Cinotti E, Fouilloux B, Perrot JL, Labeille B, Douchet C, Cambazard F. Confocal microscopy for healthy and pathological nail. J Eur Acad Dermatol Venereol. 2014;28:853–8.

18. Kadouch DJ, Leeflang MM, Elshot YS, Longo C, Ulrich M, van der Wal AC, et al. Diagnostic accuracy of confocal microscopy imaging vs. punch biopsy for diagnosing and subtyping basal cell carcinoma. J Eur Acad Dermatol Venereol. 2017;31(10):1641–8.

19. Dika E, Patrizi A, Lambertini M, Scarfì F, Fanti PA. Diagnostic accuracy of ex vivo fluorescence confocal microscopy for Mohs surgery of basal cell carcinomas: a prospective study on 753 margins. Br J Dermatol. 2019; 180:1559.

20. Pérez-Anker J, Puig S, Malvehy J. Ex vivo confocal microscopy in vertical sections and histopathological correlation (Master of Science Degree Thesis). Barcelona, Spain: University of Barcelona; 2016.

21. Bertoni L, Azzoni P, Reggiani C, Pisciotta A, Carnevale G, Chester J, et al. Ex vivo fluorescence confocal microscopy for intraoperative, real-time diagnosis of cutaneous inflammatory diseases: a preliminary study. Exp Dermatol. 2018;27(10):1152–9.

22. Hartmann D, Ruini C, Mathemeier L, Bachmann MR, Dietrich A, Ruzicka T, et al. Identification of ex-vivo confocal laser scanning microscopic features of melanocytic lesions and their histological correlates. J Biophotonics. 2017;10(1):128–42.

23. Hartmann D, Krammer S, Bachmann MR, Mathemeier L, Ruzicka T, Bagci IS, et al. Ex-vivo confocal microscopy features of cutaneous squamous cell carcinoma. J Biophotonics. 2018;11:1–7.

24. Cinotti E, Grivet D, Labeille B, Solazzi M, Bernard A, Forest F, et al. The 'tissue press': a new device to flatten fresh tissue during ex vivo confocal microscopy examination. Skin Res Technol. 2017; 23:121–4.

25. Li Y, Gonzalez S, Terwey TH, Wolchok J, Li Y, Aranda I, et al. Dual mode reflectance and fluorescence confocal laser scanning microscopy for in vivo imaging melanoma progression in murine skin. J Investig Dermatol. 2005;125(4):798–804.

26. Abeytunge S, Li Y, Larson B, Toledo-Crow R, Rajadhyaksha M. Rapid confocal imaging of large areas of excised tissue with strip mosaicing. J Biomed Optics. 2011;16(5):050504.

27. Johnson S, Rabinovitch P. Ex vivo imaging of excised tissue using vital dyes and confocal microscopy. Curr Protocols Cytometry. 2012;(61).

28. Gareau DS. Feasibility of digitally stained multimodal confocal mosaics to simulate histopathology. J Biomed Optics. 2009;14 (3):034050.

29. Bini J, Spain J, Nehal K, Hazelwood V, DiMarzio C, Rajadhyaksha M. Confocal mosaicing microscopy of human skin ex vivo: spectral analysis for digital staining to simulate histology-like appearance. J Biomedical Optics. 2011;16(7):076008.

30. Anker JP, Ribero S, Yélamos O, García A, Alos L, Alejo B, et al. Basal cell carcinoma characterisation using fusion ex vivo confocal microscopy: a promising change in conventional skin histopathology. Br J Dermatol. 2020;182(2):468–76.

31. Yélamos O, Pérez-Anker J. Avances en el manejo del cáncer cutáneo : videomosaicos y microscopía confocal de fusión. Revista chilena de dermatología. 2018;34(1):6–8.

32. Pérez-Anker J, Malvehy J, Moreno-Ramírez D. Microscopia confocal ex vivo con método de fusión y tinción digital: cambiando paradigmas en el diagnóstico histológico. Actas Dermo-Sifiliográficas.

33. Reggiani C, Pellacani G, Reggiani Bonetti L, Zanelli G, Azzoni P, Chester J, et al. An intraoperative study with ex vivo fluorescence confocal microscopy: diagnostic accuracy of the three visualization modalities. J Eur Acad Dermatol Venereol. 2021;35(1):e92–4.

34. Pérez-Anker J, Puig S, Malvehy GJ. A fast and effective option for tissue flattening: optimizing time and efficacy in ex vivo confocal microscopy. J Am Acad Dermatol Am Dermatol . 2020;82(5): e157–8.

35. Pérez-Anker J, Toll A, Puig S, Malvehy J. Six steps to reach optimal scanning in ex vivo confocal microscopy. J Am Acad Dermatol. 2021 Jan 18:S0190–9622(21)00193–6. doi: https://doi.org/10.1016/j.jaad.2021.01.044. Epub ahead of print. PMID: 33476729.

36. Sendín-Martín M, Kose K, Harris U, Rossi A, Lee E, Nehal K, et al. Complete visualization of epidermal margin during ex vivo confocal microscopy of excised tissue with 3D-mosaicking and intensity projection. J Am Acad Dermatol. 2020 May 16:S0190–9622(20)30909–9. doi: https://doi.org/10.1016/j.jaad.2020.05.044. Epub ahead of print. PMID: 32428611; https://doi.org/10.1016/j.jaad.2020.05.044

37. Toloza Salech C, Pérez-Anker J, La Rotta Higuera E, Toll A, García A, Alós LL, et al. Tinción digital en diagnóstico histológico de tumores cutáneos con microscopía confocal ex vivo de fusión. Poster presented at: 47th Congreso nacional de Dermatología y Venerología (AEDV); June 5–8, 2019; Barcelona, Spain.

38. Pérez-Anker J, Toll A, Puig S, García A, Alós Ll, Malvehy J. Real time visualization of mitosis and nuclear pleomorphism in fresh tissue using ex vivo confocal microscopy. In: Poster presented at 28th Congress of the European Academy of Dermatology and Venerology (EADV); 9–13 Oct 2019; Madrid, Spain.

39. Toloza Salech C, Malvehy J, Puig S, García A, Alós Ll, Toll A, et al. A proof of concept: digital H & E in the histological diagnosis of cutaneous tumors with ex vivo fusion confocal microscopy. In: Poster presented at: 28th congress of the european academy of dermatology and venerology (EADV); 9–13 Oct 2019; Madrid, Spain.

40. Puliatti S, Bertoni L, Pirola GM, Azzoni P, Bevilacqua L, Eissa A, et al. Ex vivo fluorescence confocal microscopy: the first application for real-time pathological examination of prostatic tissue. BJU Int. 2019;0–3.

41. Combalia M, Pérez-Anker J, García-Herrera A, Alos L, Vilaplana V, Marqués F, et al. Digitally stained confocal microscopy through deep learning. In: Proceedings of machine learning research. 2019;1–9.